JCI The Journal of Clinical Investigation

Dysregulation of PI3K and hippo signaling pathways synergistically induces chronic pancreatitis via Ctgf upregulation

Takeshi Tamura, … , Tomohide Tatsumi, Tetsuo Takehara

J Clin Invest. 2021. https://doi.org/10.1172/JCI143414.

Research In-Press Preview Gastroenterology

Graphical abstract

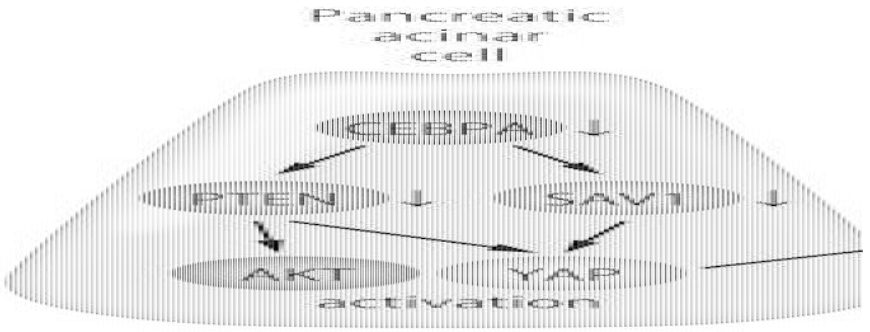

Dysregulation of PI3K and Hippo Signaling Pathways Synergistically Induces Chronic Pancreatitis via Ctgf Upregulation

Takeshi Tamura[1,*], Takahiro Kodama[1,*], Katsuhiko Sato[1], Kazuhiro Murai[1], Teppei Yoshioka[1], Minoru Shigekawa[1], Ryoko Yamada[1], Hayato Hikita[1], Ryotaro Sakamori[1], Hirofumi Akita[2], Hidetoshi Eguchi[2], Randy L. Johnson[3], Hideki Yokoi[4], Masashi Mukoyama[5], Tomohide Tatsumi[1], Tetsuo Takehara[1]

Affiliations

[1]Department of Gastroenterology and Hepatology, Osaka University Graduate School of Medicine, Suita, Osaka, Japan

[2]Department of Gastroenterological Surgery, Osaka University Graduate School of Medicine, Suita, Osaka, Japan

[3]Department of Cancer Biology, The University of Texas MD Anderson Cancer Center, Houston, Texas, 77030, USA

[4]Department of Nephrology, Kyoto University Graduate School of Medicine, Kyoto, Japan

[5]Department of Nephrology, Kumamoto University Graduate School of Medical Sciences, Kumamoto, Japan

Authorship note

* T. Tam and T. K. are co–first authors.

Grant support

This work was partially supported by a Grant-in-Aid for Scientific Research (to T. Tak) from the Ministry of Education, Culture, Sports, Science, and Technology, Japan. This work was supported by the Cancer Prevention Research Institute of Texas (CPRIT) under grant number RP180530 (R.L.J.) and the Japan Agency for Medical Research and Development (AMED) under grant number JP20fk0210074 (T.K.).

Abbreviations:

ADM, acinar-to-ductal metaplasia; Ccl2, c-c motif chemokine 2; Cebpa, CCAAT/enhancer binding protein alpha; CP, chronic pancreatitis; CPA1, carboxypeptidase A1; Col1a1, Collagen I alpha 1; Col1a2, Collagen I alpha 2; Ctgf, connective tissue growth factor; DMEM, Dulbecco's modified Eagle's medium; LATS1, large tumor suppressor kinase 1; LATS2, large tumor suppressor kinase 2; H&E, hematoxylin and eosin; PACs, pancreatic acinar cells; p-AKT, phosphorylated form of AKT; PBS, phosphate-buffered saline; PDAC, pancreatic ductal

adenocarcinoma; PDL, pancreatic duct ligation; p-LATS1/2, phosphorylated forms of large tumor suppressor kinase 1/2; PRSS1, cationic trypsinogen; PSCs, pancreatic stellate cells; Pten, Phosphatase and tensin homolog; p-YAP, phosphorylated form of YAP; Sav1, Salvador homolog 1; SPINK1, serine protease inhibitor Kazal type 1; Tgfb1, transforming growth factor-β1; Tnfa, tumor necrosis factor-α; TUNEL, terminal deoxynucleotidyl transferase-mediated deoxyuridine triphosphate nick end labeling

Correspondence

Name: Tetsuo Takehara

Address: 2-2 Yamadaoka Suita, Osaka 565-0871, Japan

e-mail: takehara@gh.med.osaka-u.ac.jp

Tel: +81-6-6879-3621

Disclosure

The authors have nothing to disclose.

Abstract

The role of PI3K and Hippo signaling in chronic pancreatitis (CP) pathogenesis is unclear. Therefore, we assessed the involvement of these pathways in CP by examining the PI3K and Hippo signaling components PTEN and SAV1, respectively. We observed significant decreases in pancreatic PTEN and SAV1 levels in 2 murine CP models: repeated caerulein injection and pancreatic ductal ligation. Additionally, pancreas-specific deletion of *Pten* and *Sav1* (DKO) induced CP in mice. Pancreatic connective tissue growth factor (CTGF) was markedly upregulated in both CP models and DKO mice, and pancreatic CCAAT/enhancer-binding protein alpha (CEBPA) expression was downregulated in the CP models. Interestingly, in pancreatic acinar cells (PACs), CEBPA knockdown reduced PTEN and SAV1 and increased CTGF levels in vitro. Furthermore, CEBPA knockdown in PACs induced acinar-to-ductal metaplasia and activation of cocultured macrophages and pancreatic stellate cells. These results were mitigated by CTGF inhibition. CP in DKO mice was also ameliorated by *Ctgf* gene deletion, and caerulein-induced CP was alleviated by antibody-mediated CTGF neutralization. Finally, we observed significantly decreased PTEN, SAV1, and CEBPA and increased CTGF levels in human CP tissues compared to nonpancreatitis tissues. Taken together, our results indicate that dysregulation of PI3K and Hippo signaling induces CP via CTGF upregulation.

Introduction

Chronic pancreatitis (CP) is characterized by continuous inflammatory destruction of the pancreas and replacement with fibrotic tissues, leading to the permanent loss of pancreatic function(1). CP is caused by heavy alcohol consumption and genetic mutations related to pancreatic digestive enzymes such as cationic trypsinogen (PRSS1), serine protease inhibitor Kazal type 1 (SPINK1), and carboxypeptidase A1 (CPA1)(2). However, 10-30% of CP cases do not have identifiable causative factors, suggesting the existence of unknown etiological factors(3). Although premature intra-acinar trypsinogen activation is a key initiating factor of pancreatitis, the pathogenesis of CP is not fully elucidated, and no effective or specific treatment exists. Therefore, further understanding of this pathogenic mechanism at the cellular and molecular levels is important to identify new therapies to prevent CP progression.

During continuous pancreatic damage, acinar cells transdifferentiate into a progenitor-like cell type with ductal characteristics. This process is called acinar-to-ductal metaplasia (ADM), and its appearance is an important morphological characteristic of CP(4). Several animal experiments have shown that ADM can develop into pancreatic intraepithelial neoplasia (PanIN) and subsequently into pancreatic ductal adenocarcinoma (PDAC)(5). Indeed, that CP is recognized to be one of the strongest risk factors for human PDAC(6). Several signaling

pathways, including the PI3K(7, 8) and Hippo signaling pathways(9), are reported to be involved in this oncogenic process. The PI3K pathway is an oncogenic signaling pathway that promotes cell proliferation and differentiation(10). Animal studies have shown that haploinsufficiency of *Pten*, which is a negative regulator of the PI3K signaling pathway, promotes PDAC development and progression in *Kras* mutant mice(7, 8). Furthermore, PTEN expression has been reported to be downregulated in most human PDACs(8), indicating that PI3K pathway activation is the driving force of PDAC development. The Hippo signaling pathway controls organ size in animals by restricting cell proliferation and promoting apoptosis, both of which are also important for tumor suppression(11). Its main component is a kinase cascade wherein mammalian STE20-like protein kinase 1 (MST1) and 2 (MST2), in complex with Salvador homolog 1 (SAV1), phosphorylate and activate the Large tumor suppressor 1 (LATS1) and 2 (LATS2) kinases, which in turn phosphorylate and inactivate the Hippo effector YES-associated protein (YAP). Hippo signaling inactivation, as represented by SAV1 downregulation or YAP activation, is correlated with poor overall survival in patients with PDAC(12-14), suggesting tumor-suppressive roles of the Hippo pathway in PDAC.

Moreover, dysregulation of the PI3K and Hippo signaling pathways has been observed in human CP(15, 16). More than half of CP patients exhibit phosphorylation of RPS6, a major downstream effector of the PI3K/AKT/mTOR pathway, in the pancreas, suggesting activation

of PI3K signaling. In addition, upregulation of YAP expression was observed in pancreatic tissue in a murine model of pancreatitis and human patients with CP, suggesting inactivation of Hippo signaling(9, 15). However, the pathological significance of these dysregulated signaling pathways in CP as well as their regulatory mechanisms are not well understood. In the present study, we found that downregulation of PTEN and SAV1 contributes to dysregulation of the PI3K and Hippo signaling pathways in murine CP models and human CP patients. We showed that mice with genetic disruption of *Pten* and *Sav1* spontaneously develop severe CP, demonstrating the importance of these signaling pathways in CP development. We also identified CCAAT/enhancer binding protein alpha (CEBPA) as the upstream regulator of both PTEN and SAV1 and showed that inactivation of CEBPA in pancreatic acinar cells (PACs) induces ADM and the activation of macrophages and pancreatic stellate cells (PSCs) via upregulation of connective tissue growth factor (CTGF). Finally, we showed that CTGF inhibition markedly ameliorates CP induced by either deletion of *Pten*/*Sav1* or repeated injection of caerulein in mice, proposing CTGF as a novel therapeutic target in CP.

Results

The expression of PTEN and SAV1 is downregulated in the pancreatic tissues of mice in two models of CP

To clarify the roles of the PI3K and Hippo signaling pathways in CP pathogenesis, we used two major murine models of CP: repeated administration of caerulein(17) and PDL(18). The pancreas atrophied in both CP models (**Supplementary Fig 1A, B**), and histological examination showed a reduced number of acinar cells and the emergence of ductal structures in the pancreas (**Fig 1A, B**). We performed immunohistochemical staining for the ADM marker SOX9 and found that the pancreas of CP model mice showed an increased number of SOX9-positive transdifferentiated ADM lesions compared to control mice (**Fig 1A, B**). CP is also characterized by chronic inflammation and fibrogenesis, which are triggered by inflammatory macrophages and PSCs, respectively(17). Indeed, both CP models showed macrophage infiltration in the pancreas, as indicated by the significant increase in *Cd68* expression, leading to marked production of inflammatory cytokines and chemokines, including *Tnfa*, *Il1b*, and *Ccl2* (**Fig 1C, D**). In addition, the expression levels of the profibrogenic *Tgfb1* gene and type I collagen (*Col1a1* and *Col1a2*) genes were significantly upregulated in the pancreas in both CP models, with widespread deposition of Sirius red-positive fibers, indicating activation of PSCs in these models (**Fig 1C, D**). Next, we examined

the expression levels of *Pten* and *Sav1*, major components of the PI3K and Hippo signaling pathways, respectively. Their mRNA levels were significantly lower in the pancreas of mice in both CP models than in those of control mice (**Fig 1E, F**). Consistent with this finding, immunohistochemical staining for PTEN and SAV1 showed that their protein levels were also significantly lower in acinar cells of mice in both CP models than in those of control mice (**Fig 1G, H**). Thus, AKT and YAP, which are the effector proteins of PI3K and Hippo signaling, respectively, were activated in the pancreas in both CP models, as demonstrated by the increase in activating phosphorylation of AKT and the decrease in inhibitory phosphorylation of YAP by western blot (WB) analysis (**Fig 1I, J**), along with the increase in phosphorylated AKT and nuclear YAP levels in acinar cells by immunohistochemistry (IHC) (**Supplementary Fig 1C, D**). We also found significant upregulation of *Ctgf*, CCN family proteins(19) and downstream transcriptional targets of the Hippo signaling pathway(20), in mice in both CP models compared to control mice (**Fig 1K**). Taken together, these results indicate that both the PI3K and Hippo signaling pathways are dysregulated in CP with the downregulation of PTEN and SAV1.

Mice with pancreas-specific loss of *Pten* and *Sav1* spontaneously develop CP

To investigate the significance of PI3K and Hippo signaling pathway dysregulation in CP, we

generated mice with pancreas-specific *Pten* and/or *Sav1* knockout (KO) (**Supplementary Fig 2A, B**). Single knockout of either *Pten* or *Sav1* in mice (*Pdx1-Cre;Pten*$^{flox/flox}$ [PTEN KO] mice and *Pdx1-Cre;Sav1*$^{flox/flox}$ [SAV1 KO] mice) did not affect pancreas weight or pancreatic histology at 6 weeks of age (**Fig 2A-C**). In sharp contrast, the pancreas of mice with deletion of both *Pten* and *Sav1* (*Pdx1-Cre;Pten*$^{flox/flox}$*;Sav1*$^{flox/flox}$ [double KO, DKO] mice) were extremely atrophied (**Fig 2A**) and weighed significantly less than those of control (*Pten*$^{flox/flox}$*;Sav1*$^{flox/flox}$ [wild-type, WT] mice) and single-knockout mice (**Fig 2B**). Histological examination showed massive loss of acinar cells, disorganized pancreatic ductal hyperplasia, the emergence of structures reminiscent of SOX9-positive ADM lesions and fibrosis in the pancreas of DKO mice (**Fig 2C**). These results indicated that mice with loss of both *Pten* and *Sav1* spontaneously develop CP. However, the presence of Glucagon-positive islet cells and the levels of serum glucose and insulin did not differ between DKO mice and the other strains of mice (**Supplementary Fig 2C, D**), suggesting that pancreatic endocrine functions were maintained in DKO mice. When we aged the mice longer, PTEN KO and SAV1 KO mice survived and developed a small amount of ADM in their pancreas at 10 months of age (**Supplementary Fig 2E**). Meanwhile, all DKO mice died by 8 weeks of age without developing PanIN or PDAC (**Supplementary Fig 2F**).

Next, we investigated the phenotypes of DKO mice at early ages after birth. The weight of

179 the pancreas increased gradually in DKO mice and did not differ from that of other mice until
180 2 weeks of age (**Supplementary Fig 2G**), excluding the possibility of failed pancreatic
181 development in DKO mice. From 2 weeks of age, the weight of the pancreas started to
182 decrease over time, and pancreatic tissues were almost completely replaced by ADM and
183 fibrotic lesions at 6 weeks of age (**Supplementary Fig 2H, I**). As expected, an increase in
184 activating phosphorylation of AKT and a decrease in inhibitory phosphorylation of YAP were
185 observed in the pancreas of DKO mice (**Fig 2D**), suggesting activation of AKT and YAP. Given
186 the stimulatory roles of AKT and YAP activation in cell proliferation, we assessed the number
187 of Ki67-positive proliferating cells in the pancreas. While a mild increase in the number of
188 Ki67-positive acinar cells was observed in PTEN KO and SAV1 KO mice compared to WT
189 mice, a massive increase in Ki67-positive ductal cells was seen in DKO mice
190 (**Supplementary Fig 2J**). The number of apoptotic acinar cells in the pancreas, as
191 determined by TUNEL staining, was increased of DKO mice compared to the other strains of
192 mice (**Supplementary Fig 2K**). Taken together, these data suggest that apoptosis of acinar
193 cells and proliferation of ductal cells may contribute to CP phenotypes in DKO mice. We then
194 examined the expression levels of inflammatory cytokines/chemokines, fibrosis-related
195 genes, and ADM-related genes in DKO mice. Similar to the pattern in both CP models, the
196 mRNA levels of *Cd68*, *Tnfa*, *Il1b*, *Ccl2*, *Tgfb1*, *Col1a1*, *Col1a2*, and *Ctgf* were all significantly

197 increased in the pancreas of DKO mice (**Fig 2E**), suggesting that pancreas-specific co-
198 deletion of PTEN and SAV1 recapitulates the CP phenotypes observed in these two major
199 CP models.
200
201 **CEBPA positively regulates PTEN and SAV1 in acinar cells, and inhibition of PTEN and**
202 **SAV1 induces ADM through CTGF upregulation in vitro**
203 We then assessed the effects of PTEN and SAV1 loss in acinar cells in vitro. To this end, we
204 knocked down PTEN or/and SAV1 in the mouse PACs tumor cell line 266-6 and found that
205 the double knockdown of PTEN and SAV1 strongly upregulated the expression of SOX9,
206 increased the expression of CTGF and decreased the inhibitory phosphorylation of YAP (**Fig**
207 **3A**). These data suggest that the inhibition of PTEN and SAV1 induces ADM in vitro,
208 recapitulating PAC phenotypes in both CP models and in DKO mice.
209 Next, we examined an upstream transcription factor (TF) that regulates *Pten* and *Sav1* in the
210 pancreas. *In silico* analysis using the TRANSFAC TF database(21) revealed that *Cebpa* was
211 the curated TF that targeted *Pten* and *Sav1*. The pancreatic expression of *Cebpa* was
212 significantly downregulated in mice in both models of experimental CP compared to control
213 mice (**Fig 3B**). We thus knocked down CEBPA in the mouse PACs tumor cell line 266-6 and
214 found that CEBPA knockdown significantly decreased the mRNA and protein levels of both

PTEN and SAV1 (**Fig 3C, D, Supplementary Fig 3A, B**), and decreased the mRNA levels of known CEBPA-target genes *Bcl-2* and *p21* (22, 23) (**Supplementary Fig 3C**), suggesting that CEBPA positively regulates PTEN and SAV1 in PACs. *In silico* analysis indicated that there are several CEBPA binding sites in their promoter regions, and a chromatin immunoprecipitation (ChIP) assay showed that CEBPA proteins bind to these regions in 266-6 cells (**Supplementary Fig 3D**), indicating that *Cebpa* transcriptionally regulates *Pten* and *Sav1* genes by binding to their promoters in pancreatic cells. CEBPA knockdown also substantially increased activating phosphorylation of AKT and decreased the inhibitory phosphorylation of YAP in 266-6 cells (**Fig 3E, Supplementary Fig 3E**). Moreover, CEBPA knockdown markedly increased SOX9 mRNA and protein levels in conjunction with CTGF upregulation in 266-6 cells (**Fig 3C, E, Supplementary Fig 3A, E**). To investigate whether the phenotypic changes induced by CEBPA knockdown in 266-6 cells are mediated by the decreased expression levels of both PTEN and SAV, we examined the effect of PTEN and SAV1 re-expression on the ADM phenotype of CEBPA-silenced cells in vitro. We confirmed that the transfection of *Pten* and *Sav1* cDNA increased the protein levels of both PTEN and SAV1 in 266-6 cells (**Supplementary Fig 3F**) and significantly suppressed the increase in the mRNA levels of *Ctgf* and *Sox9* upon CEBPA knockdown (**Supplementary Fig 3G**), suggesting that the decrease in PTEN and SAV1 resulting from CEBPA inhibition induces

ADM in vitro. Furthermore, CTGF inhibition significantly suppressed the increase in *Sox9* levels in 266-6 PACs with CEBPA knockdown (**Fig 3F, Supplementary Fig 3H**). Taken together, these data suggested that CEBPA inhibition reduced PTEN and SAV1, which induced transdifferentiation of PACs through CTGF upregulation. We also searched for upstream signals that triggered CEBPA downregulation in CP models. We found that expression levels of the *Hnf4a* and *Cebpb* genes, both of which are reported to positively regulate *Cebpa*(24, 25), significantly decreased in both CP models compared to controls (**Supplementary Fig 3I, J**).

Inhibition of PTEN and SAV1 in PACs may activate surrounding macrophages and PSCs via CTGF upregulation in vitro

To further examine the mechanisms underlying CP development in the absence of PTEN and SAV1, we focused on the interaction between PACs and macrophages/PSCs. First, we examined the expression levels of inflammatory cytokines in the macrophage cell line RAW 264.7 2 days after coculture in a Transwell system with 266-6 PACs transfected with *Cebpa* siRNA or negative control siRNA. CEBPA knockdown in acinar cells significantly increased the mRNA expression levels of *Tnfa*, *Il1b*, and *Ccl2* in the cocultured RAW 264.7 cells (**Fig 4A, Supplementary Fig 4A**). Next, we cocultured 266-6 PACs and PSCs isolated from

mouse pancreata in the Transwell coculture system. The mRNA expression levels of *Tgfb1*, *Col1a1*, and *Col1a2* were significantly higher in PSCs cocultured with 266-6 cells with CEBPA knockdown than in PSCs cocultured with 266-6 cells transfected with negative control siRNA (**Fig 4B, Supplementary Fig 4B**). These results suggest that PACs with CEBPA knockdown-mediated inhibition of PTEN and SAV1 may activate surrounding macrophages and PSCs. Interestingly, further CTGF inhibition in 266-6 PACs with CEBPA knockdown significantly suppressed the increase in the expression levels of these inflammatory cytokines in cocultured RAW 264.7 cells (**Fig 4C, Supplementary Fig 4C**) and prevented upregulation of profibrogenic genes in cocultured PSCs (**Fig 4D, Supplementary Fig 4D**), suggesting that inhibition of PTEN and SAV1 in PACs may activate surrounding macrophages and PSCs via CTGF upregulation in vitro.

CTGF produced by PACs is involved in the development of CP via pancreas-specific loss of *Pten* and *Sav1* in vivo

To investigate whether CTGF derived from PACs is involved in CP induced by deletion of *Pten* and *Sav1* in mice, we generated mice with pancreas-specific triple knockout of *Pten*, *Sav1*, and *Ctgf* (*Pdx1-Cre;Pten*$^{flox/flox}$*;Sav1*$^{flox/flox}$*;Ctgf*$^{flox/flox}$) (triple KO, TKO) mice and compared pancreatic phenotypes among WT, DKO and TKO mice. We first confirmed that

the levels of *Pten*, *Sav1*, and *Ctgf* were significantly decreased in the pancreas of TKO mice compared to WT mice (**Fig 5A**). The weight of the pancreas was significantly increased in TKO mice compared to DKO mice (**Fig 5B, C**). Importantly, histological analysis showed that the acinar cell loss, ADM formation and fibrosis observed in DKO mice were mitigated in TKO mice (**Fig 5D, E**). In addition, the pancreatic expression levels of *Cd68*, together with those of *Tnfa*, *Il1b*, and *Ccl2*, were significantly lower in TKO mice than in DKO mice (**Fig 5F**). Similarly, *Ctgf* deletion significantly suppressed the upregulation of *Tgfb1*, *Col1a1*, and *Col1a2* expression observed in DKO mice (**Fig 5F**). While all DKO mice died early (**Supplementary Fig 2F**), some of the TKO mice survived to reach 10 months of age without developing PanIN or PDAC (**Supplementary Fig 5A**). Taken together, these results indicate that in the absence of PTEN and SAV1, CTGF in PACs promotes CP development in mice via the acceleration of ADM formation and activation of surrounding macrophages and PSCs.

CTGF inhibition ameliorates CP by alleviating inflammation, fibrogenesis and ADM formation in vivo

To explore the therapeutic potential of targeting CTGF in CP, we treated mice with caerulein-induced CP with either FG-3154, an anti-CTGF neutralizing antibody, or control IgG. The therapeutic protocol is shown in Fig 6A. Compared to control IgG treatment, FG-3154

287 treatment significantly alleviated the pancreatic weight loss caused by repeated caerulein
288 injection (**Fig 6B, C**). Histologically, while CP post-treatment phenotypes were comparable
289 to pretreatment phenotypes in the control IgG group (**Fig 6D, E**), the anti-CTGF neutralizing
290 antibody treatment alleviated CP phenotypes (**Fig 6D, E**). Furthermore, compared to control
291 IgG treatment, FG-3154 treatment significantly suppressed the upregulation of *Cd68*, *Tnfa*,
292 *Il1b*, *Ccl2*, *Tgfb1*, *Col1a1*, and *Col1a2* expression caused by repeated caerulein injection
293 (**Fig 6F**). Taken together, our data show that CTGF inhibition suppresses CP progression by
294 alleviating inflammation, fibrogenesis and ADM formation, thereby suggesting that targeting
295 CTGF is a novel potential therapeutic approach for CP.
296
297 **Chronic pancreatitis tissues exhibit lower CEBPA, PTEN and SAV1 levels and higher**
298 **CTGF levels than nonpancreatitis tissues from humans**
299 Finally, we assessed the clinical significance of our findings using chronic pancreatitis tissues
300 and nonpancreatitis tissues from patients. To this end, we first histopathologically evaluated
301 obstructive pancreatitis tissues and nonpancreatitis tissues from the same patients. Among
302 patients who underwent surgical resection of the pancreas due to PDAC development at the
303 pancreatic body, 6 exhibited obstructive pancreatitis on the tail side but not the head side.
304 Chronic pancreatitis tissues exhibited decreased numbers of PACs, increased areas of

fibrosis, and SOX9-positive ADM lesions compared to nonpancreatitis tissues in these patients (**Fig 7A, B**). We then performed immunohistochemical staining for CEBPA, PTEN, SAV1, p-AKT, YAP, and CTGF in the pancreatic tissues. The expression levels of PTEN, SAV1, and CEBPA were significantly lower in chronic pancreatitis tissues than in nonpancreatitis tissues (**Fig 7C, D**). In contrast, p-AKT, nuclear YAP, and CTGF levels were significantly higher in chronic pancreatitis tissues than in nonpancreatitis tissues (**Fig 7C, D**). Next, we also performed the same histopathological analyses using pancreatic tissues from chronic pancreatitis patients and normal pancreatic tissues from pancreatic neuroendocrine tumor patients. Similar to the obstructive pancreatitis tissues, chronic pancreatitis tissues showed significantly lower levels of PTEN, SAV1, and CEBPA and higher levels of p-AKT, nuclear YAP, and CTGF than those in normal pancreatic tissues (**Fig 7E, Supplementary Fig 6A-C**). Collectively, these data suggest that dysregulation of the CEBPA-PTEN/SAV1-CTGF axis might be involved in the development of CP in humans.

Discussion

In this study, we focused on the PI3K and Hippo signaling pathways, both of which are important for PDAC development, and provided novel, important in vivo experimental evidence that dysregulation of these pathways synergistically contributes to CP pathogenesis. Additionally, we found that downregulation of PTEN and SAV1 are partially responsible for dysregulation of these pathways and occur in human CP patients, supporting the clinical relevance of our findings. Recently, crosstalk between the PI3K and Hippo signaling pathways has been shown to be involved in organ development as well as in the pathophysiology of various diseases(26-29). During organ development, YAP downregulates PTEN via miR-29 induction and activates PI3K-mTOR signaling, regulating organ size(30). Inversely, PTEN inactivation suppresses the MOB1-LATS1/2 interaction, leading to YAP activation, which accelerates gastric tumorigenesis(28). Therefore, these pathways are regulated bidirectionally at the molecular level. Moreover, we previously showed that simultaneous loss of PTEN and SAV1 in the liver induces synergistic activation of liver progenitor cells, leading to early and aggressive hepatocarcinogenesis(29), indicating the presence of synergistic crosstalk between these pathways. In the present study, we observed that single deletion of either *Pten* or *Sav1* did not result in any pancreatic phenotype, but dual deletion resulted in rapid disruption of exocrine homeostasis, leading to CP development.

Therefore, synergistic crosstalk between the PI3K and Hippo signaling pathways also exists in the pancreas and plays a critical role in CP pathogenesis. At the cellular and molecular levels, we found that either SAV1 or PTEN inhibition slightly reduced phosphorylation of LATS1/2, leading to only mild YAP activation in PACs. In contrast, dual deletion of SAV1 and PTEN almost completely eliminated the phosphorylation of LATS1/2 and thus strongly activated YAP, inducing ADM in these cells. These data suggested that crosstalk between PTEN and SAV1 affected the activation of LATS1/2-YAP signaling in PACs. This YAP activity was comparable to that acquired through LATS1/2 inhibition (**Fig 3A**). This may reflect the previous report that mice with deletion of both *Lats1/2* spontaneously develop chronic pancreatitis similar to that in our DKO mice(31).

In an aim to identify the upstream regulator of the PI3K and Hippo signaling pathways in acinar cells, we found that the expression level of CEBPA decreased along with the expression levels of both PTEN and SAV1 in the pancreas of mice with CP induced via either of two different methods. CEBPA, a member of the C/EBP family of TFs, arrests cellular proliferation and drives terminal differentiation in a variety of adult tissues, including those composed of granulocytes, adipocytes, hepatocytes, pneumocytes, and osteoclasts(23, 32, 33). In addition, CEBPA is indispensable for maintaining postnatal systemic energy

359 homeostasis and lipid storage(34). The *CEBPA* gene has been reported to act as a tumor
360 suppressor in many tumor types and to be epigenetically silenced in pancreatic cancer
361 cells(23, 35). On the other hand, the functional role of CEBPA in PACs remains unclear.
362 *CEBPA* directly controls many genes involved in the cell cycle and cell proliferation, such as
363 *CDKN1A*, *E2F1* and *MYC*, as well as a variety of metabolic genes(23, 34). In this study, we
364 demonstrated for the first time that CEBPA positively regulates PTEN and SAV1 in PACs and
365 maintains their integrity by preventing their transformation into ductal cells. Considering that
366 CEBPA positively regulates two major tumor suppressors in the pancreas, further examining
367 the involvement of this tumor-suppressive link in PDAC development would be interesting.
368
369 We focused on CTGF as the critical downstream mediator of the PI3K and Hippo pathways
370 during CP development. Several studies have shown that CTGF acts as a profibrogenic
371 factor and activates fibroblasts in various organs including the pancreas, facilitating fibroblast
372 proliferation and collagen production, which promote organ fibrogenesis(15, 36-38). CTGF
373 is considered to be produced mainly by fibroblasts, but recent reports have shown that CTGF
374 secreted from epithelial cells also contributes significantly to disease pathogenesis(39, 40).
375 We and others have reported that CTGF secreted from hepatocytes may contribute to liver
376 fibrogenesis via activation of nearby hepatic stellate cells (HSCs)(39, 41, 42). In the pancreas,

Charrier A et al. reported that CTGF was produced from PACs, as well as PSCs, under ethanol stimulus, suggesting the potential involvement of PAC-derived CTGF in CP development (43). In our current study, we found that in vitro, PAC-derived CTGF promotes ductal metaplasia and activates surrounding macrophages and PSCs, suggesting a novel pleiotropic function of PAC-derived CTGF during CP development in cell-autonomous and cell-heteronomous manners. Furthermore, we demonstrated for the first time that PAC-derived CTGF is involved in ADM formation, inflammation, and fibrogenesis during CP in vivo. These results suggest that PAC-derived CTGF is pivotal in the development of CP.

CTGF expression has previously been reported to be increased in human CP(44). However, its regulatory mechanism and pathological significance remain unclear. In this study, we showed that genetic disruption of *Pten* and *Sav1* synergistically upregulates CTGF expression in the pancreas of mice with CP, providing the first demonstration of the regulatory link between PTEN/SAV1 and CTGF in CP. Consistent with this finding, we also observed that in human obstructive pancreatitis, the expression of PTEN and SAV1 was decreased, whereas that of CTGF was increased(44), suggesting the existence of this regulatory link in human CP. More importantly, we demonstrated the in vivo therapeutic efficacy of blocking CTGF in mouse models of both genetically and chemically induced CP. Liu J et al. also very

recently showed the antifibrotic effects of an anti-CTGF neutralizing antibody in a different animal model of CP, *Lats1/2* double knockout mice(31). Taken together, the results of our studies highlight CTGF as a promising novel therapeutic target for CP. Moreover, we showed that in the caerulein-induced murine model of CP, treatment with an anti-CTGF neutralizing antibody alleviated inflammation, fibrosis, and ADM, all of which are known to induce PDAC development. Therefore, amelioration of inflammation and fibrosis during CP via CTGF inhibition might also prevent CP-induced pancreatic carcinogenesis, and this important beneficial effect needs further assessment.

In conclusion, our study revealed the important molecular mechanism of CP development, i.e., that dysregulation of PI3K and Hippo signaling in PACs promotes ADM, which is followed by inflammation with macrophage infiltration and fibrosis with PSC activation, resulting in rapid development of CP. Furthermore, we identified CTGF as the downstream effector of PI3K and Hippo signaling responsible for CP progression and provided robust evidence that CTGF inhibition reduces the severity of CP in vivo. These results indicate that targeting CTGF could be an effective therapeutic strategy for CP.

Methods

Mice

C57BL/6J and *Pten*$^{flox/+}$ mice were purchased from Jackson Laboratory. *Pdx1-Cre* transgenic mice was obtained from the Mouse Models of Human Cancer Consortium (National Cancer Institute–Frederick, Bethesda, Maryland). *Sav1*$^{flox/flox}$ and *Ctgf*$^{flox/flox}$ mice were generated as previously described(45, 46). To establish the model of caerulein-induced CP, 6-week-old C57BL/6J mice received caerulein (solubilized in PBS at a final concentration of 10 μg/ml and injected intraperitoneally at a dose of 50 μg/kg) every hour for six hours three times per week for 7 weeks. Controls received PBS injections. To establish the model of pancreatic duct ligation (PDL)-induced CP, 6-week-old C57BL/6J mice were subjected to PDL as previously described(18). Controls were subjected to surgery without duct ligation. The mice were sacrificed at the indicated time points. To generate *Pdx1-Cre;Pten*$^{flox/flox}$*;Sav1*$^{flox/flox}$ mice, *Pten*$^{flox/+}$ mice or *Sav1*$^{flox/flox}$ mice were first crossed with *Pdx1-Cre* mice to generate *Pdx1-Cre;Pten*$^{flox/+}$ mice *or Pdx1-Cre;Sav1*$^{flox/+}$ mice. The resulting mice were then intercrossed to generate *Pten*$^{flox/flox}$*;Sav1*$^{flox/flox}$ (WT) mice, *Pdx1-Cre;Pten*$^{flox/flox}$ (PTEN KO) mice, *Pdx1-Cre;Sav1*$^{flox/flox}$ (SAV1 KO) mice, and *Pdx1-Cre;Pten*$^{flox/flox}$*;Sav1*$^{flox/flox}$ (DKO) mice. Additionally, the resulting mice were crossed with *Ctgf*$^{flox/flox}$ mice to generate *Pdx1-Cre;Pten*$^{flox/flox}$*;Sav1*$^{flox/flox}$*;Ctgf*$^{flox/flox}$ (TKO) mice. All the genetically engineered mouse

models were followed into adulthood.

Blood and tissue preparation

All mice were sacrificed under pentobarbital anesthesia, and peripheral blood and samples of the pancreas were collected for study. Harvested blood was centrifuged at 13,500 rpm for 10 min to separate the serum. Each pancreas was rapidly removed, weighed, and either snap-frozen for molecular analysis or fixed with 10% neutral phosphate-buffered formalin for histological analysis.

Histological and immunohistochemical analyses

Pancreatic tissues were stained with a standard hematoxylin and eosin (H&E) preparation. Sirius red staining was performed to assess the degree of pancreatic fibrosis. To detect apoptotic cells, a terminal deoxynucleotidyl transferase-mediated deoxyuridine triphosphate nick end labeling (TUNEL) assay was performed with an ApopTag Peroxidase In Situ Apoptosis Detection Kit according to the manufacturer's instructions (Merck KGaA, Darmstadt, Germany). Immunohistochemical analyses of paraffin-embedded pancreatic tissues were performed using antibodies specific for PTEN, SOX9, p-AKT, YAP, Glucagon, Ki67, CEBPA, CTGF (Abcam, Cambridge, UK), and SAV1 (Novus Biologicals, CO, USA).

Immunostained tissues were imaged with a SLIDEVIEW VS200 (Olympus, Tokyo, Japan), and the immunostaining intensity of each PAC was quantified with ImageJ software (National Institutes of Health, Bethesda, Maryland, USA). The detailed antibody information is described in Supplementary Table 1.

Biochemical Analysis

Mouse serum glucose levels were enzymatically measured at the Oriental Kobo Life Science Laboratory. Mouse serum insulin levels were measured using an ELISA kit (Morinaga Institute of Biological Science, Yokohama, Japan).

RNA isolation and quantitative PCR

The total RNA was extracted from cell lines or pancreatic tissues using an RNeasy Mini Kit (QIAGEN, Hilden, Germany) according to the manufacturer's instructions, and cDNA was synthesized using reverse transcription as previously described(47). Quantitative PCR was performed in a Quant Studio 6 Flex Real-Time PCR System (Thermo Fisher Scientific, MA, USA) with TaqMan probes. Relative gene expression levels were determined by the ΔΔCT method and normalized to those of *Actb*. The detailed probe (Thermo Fisher Scientific) information is described in Supplementary Table 2.

Western blot analysis

Samples of pancreatic tissues or harvested cells were lysed in lysis buffer (1% Nonidet P-40, 0.5% sodium deoxycholate, 0.1% sodium dodecyl sulfate, protease inhibitor cocktail (Nacalai Tesque), phosphatase inhibitor cocktail (Nacalai Tesque), and PBS [pH 7.4]). Equal amounts of protein were electrophoretically separated and subjected to western blotting. The following antibodies were used as primary antibodies: anti-AKT, anti-p-AKT, anti-YAP, anti-p-YAP, anti-CEBPA, anti-SOX9, anti-LATS1, anti-PTEN, anti-SAV1 (all from Cell Signaling Technology, MA, USA), anti-CTGF (Abcam), anti-LATS2 and anti-p-LATS1/2 (Invitrogen, MA, USA), and anti-ACTB (Sigma-Aldrich, MO, USA). The detailed antibody information is described in Supplementary Table 1.

Cell culture

The mouse PACs tumor cell line 266-6 and the mouse macrophage cell line RAW 264.7 were obtained from the American Type Culture Collection (ATCC) cell bank and cultured in Dulbecco's modified Eagle's medium (DMEM; Nacalai Tesque, Kyoto, Japan) containing 10% heat-inactivated fetal calf serum, 100 U/ml penicillin and 100 μg/ml streptomycin. Mouse PSCs were isolated from C57BL/6 mice by a previously described method with

modifications(48). All cells were maintained at 37°C in a humidified atmosphere containing 5% CO_2. All cells were confirmed to be pathogen- and mycoplasma-free.

Chromatin Immunoprecipitation Assay

First, 266-6 cells were prepared by using the SimpleChIP Plus Enzymatic Chromatin IP kit (#9005; Cell Signaling Technology). Nuclear extracts from 266-6 cells were cross-linked by the addition of formaldehyde, sonicated, and used for immunoprecipitation with the CEBPA rabbit polyclonal antibody (#18311-1-AP; Proteintech, IL, USA). Reverse cross-linked chromatin immunoprecipitation DNA samples were subjected to real-time PCR using the oligonucleotides specific to promoter regions of the murine *Pten* gene, 5′-AGGAACAGCTTGGGGACTCT-3′ (S) and 5′-CCGGATCGGAGCAGAGAATAG-3′ (AS), and those of the murine *Sav1* gene, 5′-TCTGGTGCTCAAAGGCTTCAA-3′ (S) and 5′-TCCGCGCTTTCGGATTAAA-3′ (AS), which were synthesized by Integrated DNA Technologies (IDT, IA, USA).

Cell transfection with small interfering RNA (siRNA)

Silencer Select siRNAs against mouse *Pten*, *Sav1*, *Lats1*, *Lats2*, *Cebpa* and *Ctgf* were designed and synthesized by Thermo Fisher Scientific. We used 2 independent siRNAs

against *Cebpa* (#1-2) and *Ctgf* (#1-2). Cells were transfected using the reverse transfection method. First, 266-6 cells were transfected with siRNAs (10 nM) using Lipofectamine RNAiMAX (Thermo Fisher Scientific) according to the manufacturer's instructions. In brief, the 266-6 cells were plated in 12-well plates, and either Silencer Select negative control siRNAs or target siRNAs mixed with Lipofectamine RNAiMAX were added to the plates on the same day. Three to five days after transfection, the cells were used for experiments. The detailed siRNA information is described in Supplementary Table 3.

Plasmid Construction and Transfection

Pten and *Sav1* expression vectors and 266-6 cells were used to establish transfectants of both of these genes. The full-length mouse *Pten* cDNA was synthesized by Integrated DNA Technologies. The LentiCas9-Blast plasmid (#52962; Addgene, MA, USA) was cut with BamHI and XbaI restriction enzymes, and then the *Pten* cDNA was inserted into the plasmid. Additionally, the *Sav1* expression vector was purchased from origene (#MR206033L4; origene, MD, USA). Accordingly, the 266-6 cells were then transfected with both the *Pten* cDNA insert vector and *Sav1* expression vector or control vector and Lipofectamine 2000 (#11668019; Thermo Fisher Scientific). Puromycin and Blasticidin were used for the selection of both *Pten*- and *Sav1*-expressing transfectants.

Transwell assay

RAW 264.7 cells or PSCs were cultured in the bottom compartment of a 12-well Transwell cell culture system (pore size 3.0 μm; Corning, NY, USA), and 266-6 cells transfected with either Silencer Select negative control siRNAs or target siRNAs were cultured on the membranes of the Transwell cell culture inserts. After 2 days of coculture in the Transwell system, the RAW 264.7 cells or PSCs were used for experiments.

Administration of FG-3154

FG-3154, a fully human neutralizing mAb recognizing CTGF and a human control IgG were provided by FibroGen (San Francisco, USA). CP was induced by intraperitoneal injection of caerulein (50 μg/kg) three days per week for seven weeks. During the final 2 weeks of caerulein injection, 40 mg/kg FG-3154 or control IgG was administered twice weekly by intraperitoneal injection.

Human samples

Six pancreas samples of obstructive pancreatitis tissues and nonpancreatitis tissues were collected from patients with pancreatic body cancer who underwent distal pancreatectomy.

In addition, six pancreas samples of chronic pancreatitis tissues were collected from 3 patients with alcoholic chronic pancreatitis, 2 patients with tumor-forming pancreatitis, and 1 patient with familial pancreatitis, all of whom underwent pancreaticoduodenectomy or distal pancreatectomy. Six samples of normal pancreatic tissues were collected from patients with pancreatic neuroendocrine tumors who underwent pancreaticoduodenectomy or distal pancreatectomy. All surgeries were performed at the Department of Gastroenterological Surgery, Osaka University Graduate School of Medicine, between February 2011 and April 2018.

Statistical analysis

Statistical analyses were performed using Prism 9.0.1 software (GraphPad, CA, USA). Data are presented as the means ± standard deviation errors of the mean (SDs). Student's t-test was used to evaluate differences between two groups. One-way analysis of variance (ANOVA) with Tukey's post hoc test was used to compare differences among three or more groups. The survival data were analyzed using the log-rank test. A P value < 0.05 was considered significant.

Study approval

All animal experimental procedures were performed in accordance with the Osaka University guidelines for animal experiments and approved by the Ethics Committee of Osaka University Graduate School of Medicine. The use of resected human samples was approved by the Ethics Committee of Osaka University Graduate School of Medicine (Protocol number: 17160) and written informed consent was received from all patients. The study design was consistent with the principles of the Declaration of Helsinki.

Author Contributions

Conceptualization, writing, review, and editing: T. Tam., T. K., R. L. J., and T. Tak. Data curation and formal analysis: T. Tam., T. K., and T. Tak. Methodology: T. Tam., T. K., M. S., H. H., and T. Tak. Funding acquisition: T. K., and T. Tak. Project administration and supervision: T. Tak. Resources: K. S., K. M., T. Y., R. Y., R. S., H. A., H. E., H. Y., M. M., and T. Tat. The order of first authorship was determined by levels of contribution to manuscript writing.

Acknowledgments

This work was partially supported by a Grant-in-Aid for Scientific Research (to T. Takehara) from the Ministry of Education, Culture, Sports, Science, and Technology, Japan. The authors thank FibroGen for kindly providing the anti-CTGF neutralizing antibody FG-3154.

References

1. Kloppel G. Chronic pancreatitis, pseudotumors and other tumor-like lesions. *Mod Pathol.* 2007;20 Suppl 1:S113-31.

2. Masamune A, Kotani H, Sorgel FL, Chen JM, Hamada S, Sakaguchi R, et al. Variants That Affect Function of Calcium Channel TRPV6 Are Associated With Early-onset Chronic Pancreatitis. *Gastroenterology.* 2020.

3. Lew D, Afghani E, and Pandol S. Chronic Pancreatitis: Current Status and Challenges for Prevention and Treatment. *Dig Dis Sci.* 2017;62(7):1702-12.

4. Lowenfels AB, Maisonneuve P, Cavallini G, Ammann RW, Lankisch PG, Andersen JR, et al. Pancreatitis and the risk of pancreatic cancer. International Pancreatitis Study Group. *N Engl J Med.* 1993;328(20):1433-7.

5. Zhu L, Shi G, Schmidt CM, Hruban RH, and Konieczny SF. Acinar cells contribute to the molecular heterogeneity of pancreatic intraepithelial neoplasia. *Am J Pathol.* 2007;171(1):263-73.

6. Pinho AV, Chantrill L, and Rooman I. Chronic pancreatitis: a path to pancreatic cancer. *Cancer Lett.* 2014;345(2):203-9.

7. Hill R, Calvopina JH, Kim C, Wang Y, Dawson DW, Donahue TR, et al. PTEN loss accelerates KrasG12D-induced pancreatic cancer development. *Cancer Res.*

2010;70(18):7114-24.

8. Ying H, Elpek KG, Vinjamoori A, Zimmerman SM, Chu GC, Yan H, et al. PTEN is a major tumor suppressor in pancreatic ductal adenocarcinoma and regulates an NF-kappaB-cytokine network. *Cancer Discov.* 2011;1(2):158-69.

9. Gruber R, Panayiotou R, Nye E, Spencer-Dene B, Stamp G, and Behrens A. YAP1 and TAZ Control Pancreatic Cancer Initiation in Mice by Direct Up-regulation of JAK-STAT3 Signaling. *Gastroenterology.* 2016;151(3):526-39.

10. Hay N, and Sonenberg N. Upstream and downstream of mTOR. *Genes Dev.* 2004;18(16):1926-45.

11. Zhao B, Tumaneng K, and Guan KL. The Hippo pathway in organ size control, tissue regeneration and stem cell self-renewal. *Nat Cell Biol.* 2011;13(8):877-83.

12. Ansari D, Ohlsson H, Althini C, Bauden M, Zhou Q, Hu D, et al. The Hippo Signaling Pathway in Pancreatic Cancer. *Anticancer Res.* 2019;39(7):3317-21.

13. Wang L, Wang Y, Li PP, Wang R, Zhu Y, Zheng F, et al. Expression profile and prognostic value of SAV1 in patients with pancreatic ductal adenocarcinoma. *Tumour Biol.* 2016.

14. Wang L, Wang M, Hu C, Li P, Qiao Y, Xia Y, et al. Protein salvador homolog 1 acts as a tumor suppressor and is modulated by hypermethylation in pancreatic ductal adenocarcinoma. *Oncotarget.* 2017;8(38):62953-61.

15. Morvaridi S, Dhall D, Greene MI, Pandol SJ, and Wang Q. Role of YAP and TAZ in pancreatic ductal adenocarcinoma and in stellate cells associated with cancer and chronic pancreatitis. *Sci Rep.* 2015;5:16759.

16. Bellizzi AM, Bloomston M, Zhou XP, Iwenofu OH, and Frankel WL. The mTOR pathway is frequently activated in pancreatic ductal adenocarcinoma and chronic pancreatitis. *Appl Immunohistochem Mol Morphol.* 2010;18(5):442-7.

17. Xue J, Sharma V, Hsieh MH, Chawla A, Murali R, Pandol SJ, et al. Alternatively activated macrophages promote pancreatic fibrosis in chronic pancreatitis. *Nat Commun.* 2015;6:7158.

18. Xu X, D'Hoker J, Stangé G, Bonné S, De Leu N, Xiao X, et al. Beta cells can be generated from endogenous progenitors in injured adult mouse pancreas. *Cell.* 2008;132(2):197-207.

19. Lau LF. Cell surface receptors for CCN proteins. *J Cell Commun Signal.* 2016;10(2):121-7.

20. Piccolo S, Dupont S, and Cordenonsi M. The biology of YAP/TAZ: hippo signaling and beyond. *Physiol Rev.* 2014;94(4):1287-312.

21. Matys V, Kel-Margoulis OV, Fricke E, Liebich I, Land S, Barre-Dirrie A, et al. TRANSFAC and its module TRANSCompel: transcriptional gene regulation in eukaryotes. *Nucleic*

Acids Res. 2006;34(Database issue):D108-10.

22. Dooher JE, Paz-Priel I, Houng S, Baldwin AS, and Friedman AD. C/EBPα, C/EBPα oncoproteins, or C/EBPβ preferentially bind NF-κB p50 compared with p65, focusing therapeutic targeting on the C/EBP:p50 interaction. *Mol Cancer Res.* 2011;9(10):1395-405.

23. Koschmieder S, Halmos B, Levantini E, and Tenen DG. Dysregulation of the C/EBPalpha differentiation pathway in human cancer. *J Clin Oncol.* 2009;27(4):619-28.

24. Wiwi CA, Gupte M, and Waxman DJ. Sexually dimorphic P450 gene expression in liver-specific hepatocyte nuclear factor 4alpha-deficient mice. *Mol Endocrinol.* 2004;18(8):1975-87.

25. Alonso-Vale MI, Peres SB, Vernochet C, Farmer SR, and Lima FB. Adipocyte differentiation is inhibited by melatonin through the regulation of C/EBPbeta transcriptional activity. *J Pineal Res.* 2009;47(3):221-7.

26. Fu Y, Sun S, Sun H, Peng J, Ma X, Bao L, et al. Scutellarin exerts protective effects against atherosclerosis in rats by regulating the Hippo-FOXO3A and PI3K/AKT signaling pathways. *J Cell Physiol.* 2019;234(10):18131-45.

27. Zhao Y, Montminy T, Azad T, Lightbody E, Hao Y, SenGupta S, et al. PI3K Positively Regulates YAP and TAZ in Mammary Tumorigenesis Through Multiple Signaling

683 Pathways. *Mol Cancer Res.* 2018;16(6):1046-58.

684 28. Xu W, Yang Z, Xie C, Zhu Y, Shu X, Zhang Z, et al. PTEN lipid phosphatase inactivation
685 links the hippo and PI3K/Akt pathways to induce gastric tumorigenesis. *J Exp Clin Cancer*
686 *Res.* 2018;37(1):198.

687 29. Kodama T, Yi J, Newberg JY, Tien JC, Wu H, Finegold MJ, et al. Molecular profiling of
688 nonalcoholic fatty liver disease-associated hepatocellular carcinoma using SB
689 transposon mutagenesis. *Proc Natl Acad Sci U S A.* 2018;115(44):E10417-E26.

690 30. Tumaneng K, Schlegelmilch K, Russell RC, Yimlamai D, Basnet H, Mahadevan N, et al.
691 YAP mediates crosstalk between the Hippo and PI(3)K-TOR pathways by suppressing
692 PTEN via miR-29. *Nat Cell Biol.* 2012;14(12):1322-9.

693 31. Liu J, Gao M, Nipper M, Deng J, Sharkey FE, Johnson RL, et al. Activation of the intrinsic
694 fibroinflammatory program in adult pancreatic acinar cells triggered by Hippo signaling
695 disruption. *PLoS Biol.* 2019;17(9):e3000418.

696 32. Rishi V, Bhattacharya P, Chatterjee R, Rozenberg J, Zhao J, Glass K, et al. CpG
697 methylation of half-CRE sequences creates C/EBPalpha binding sites that activate some
698 tissue-specific genes. *Proc Natl Acad Sci U S A.* 2010;107(47):20311-6.

699 33. Jules J, Chen W, Feng X, and Li YP. CCAAT/Enhancer-binding Protein alpha
700 (C/EBPalpha) Is Important for Osteoclast Differentiation and Activity. *J Biol Chem.*

2016;291(31):16390-403.

34. Flodby P, Barlow C, Kylefjord H, Ahrlund-Richter L, and Xanthopoulos KG. Increased hepatic cell proliferation and lung abnormalities in mice deficient in CCAAT/enhancer binding protein alpha. *J Biol Chem.* 1996;271(40):24753-60.

35. Kumagai T, Akagi T, Desmond JC, Kawamata N, Gery S, Imai Y, et al. Epigenetic regulation and molecular characterization of C/EBPalpha in pancreatic cancer cells. *Int J Cancer.* 2009;124(4):827-33.

36. Zhang Z, Wang J, Chen Y, Suo L, Chen H, Zhu L, et al. Activin a promotes myofibroblast differentiation of endometrial mesenchymal stem cells via STAT3-dependent Smad/CTGF pathway. *Cell Commun Signal.* 2019;17(1):45.

37. Dorn LE, Petrosino JM, Wright P, and Accornero F. CTGF/CCN2 is an autocrine regulator of cardiac fibrosis. *J Mol Cell Cardiol.* 2018;121:205-11.

38. Charrier A, and Brigstock DR. Regulation of pancreatic function by connective tissue growth factor (CTGF, CCN2). *Cytokine Growth Factor Rev.* 2013;24(1):59-68.

39. Kodama T, Takehara T, Hikita H, Shimizu S, Shigekawa M, Tsunematsu H, et al. Increases in p53 expression induce CTGF synthesis by mouse and human hepatocytes and result in liver fibrosis in mice. *J Clin Invest.* 2011;121(8):3343-56.

40. Makino Y, Hikita H, Kodama T, Shigekawa M, Yamada R, Sakamori R, et al. CTGF

719 Mediates Tumor-Stroma Interactions between Hepatoma Cells and Hepatic Stellate Cells
720 to Accelerate HCC Progression. *Cancer Res.* 2018;78(17):4902-14.
721 41. Rachfal AW, and Brigstock DR. Connective tissue growth factor (CTGF/CCN2) in hepatic
722 fibrosis. *Hepatol Res.* 2003;26(1):1-9.
723 42. Gressner OA, and Gressner AM. Connective tissue growth factor: a fibrogenic master
724 switch in fibrotic liver diseases. *Liver Int.* 2008;28(8):1065-79.
725 43. Charrier A, Chen R, Kemper S, and Brigstock DR. Regulation of pancreatic inflammation
726 by connective tissue growth factor (CTGF/CCN2). *Immunology.* 2014;141(4):564-76.
727 44. di Mola FF, Friess H, Martignoni ME, Di Sebastiano P, Zimmermann A, Innocenti P, et al.
728 Connective tissue growth factor is a regulator for fibrosis in human chronic pancreatitis.
729 *Ann Surg.* 1999;230(1):63-71.
730 45. Lu L, Li Y, Kim SM, Bossuyt W, Liu P, Qiu Q, et al. Hippo signaling is a potent in vivo
731 growth and tumor suppressor pathway in the mammalian liver. *Proc Natl Acad Sci U S A.*
732 2010;107(4):1437-42.
733 46. Toda N, Mori K, Kasahara M, Ishii A, Koga K, Ohno S, et al. Crucial Role of Mesangial
734 Cell-derived Connective Tissue Growth Factor in a Mouse Model of Anti-Glomerular
735 Basement Membrane Glomerulonephritis. *Sci Rep.* 2017;7:42114.
736 47. Kodama T, Takehara T, Hikita H, Shimizu S, Li W, Miyagi T, et al. Thrombocytopenia

exacerbates cholestasis-induced liver fibrosis in mice. *Gastroenterology.* 2010;138(7):2487-98, 98.e1-7.

48. Leal AS, Misek SA, Lisabeth EM, Neubig RR, and Liby KT. The Rho/MRTF pathway inhibitor CCG-222740 reduces stellate cell activation and modulates immune cell populations in Kras. *Sci Rep.* 2019;9(1):7072.

FIGURE LEGENDS

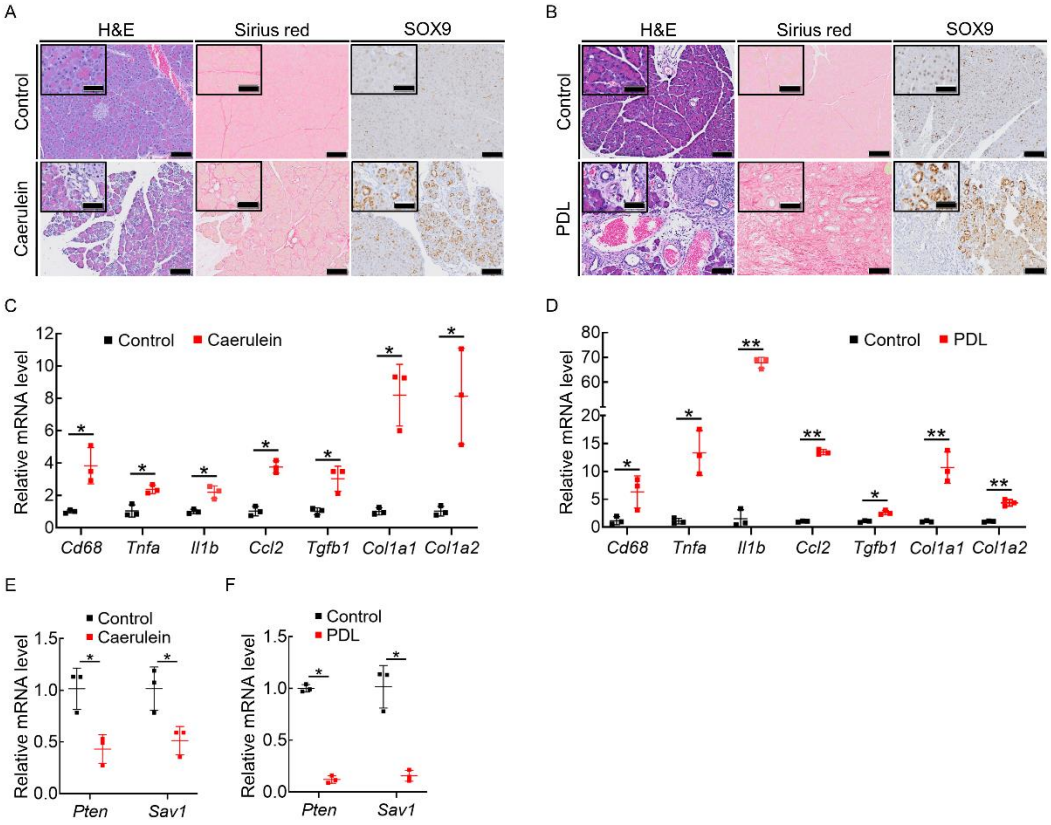

Figure 1

The expression of PTEN and SAV1 is downregulated in the pancreatic tissues of mice in two models of CP.

(A-B) Representative images of H&E, Sirius red, and SOX9 staining of pancreatic tissue in mice after repeated caerulein or vehicle (control) injection **(A)** and in mice subjected to PDL surgery or sham surgery **(B)**. **(C-D)** *Cd68*, *Tnfa*, *Il1b*, *Ccl2*, *Tgfb1*, *Col1a1*, and *Col1a2* mRNA levels in pancreatic tissue in mice after repeated caerulein injection **(C)** and in mice subjected to PDL surgery **(D)**. **(E-F)** *Pten* and *Sav1* mRNA levels in pancreatic tissue in mice after repeated caerulein injection **(E)** and in mice subjected to PDL surgery **(F)**. All data are presented as the means ± SDs of results for 3 mice per group. Student's t-test was used to evaluate differences between two groups. * $p < 0.05$ and ** $p < 0.005$. Scale bars: 100 μm and 50 μm (insets).

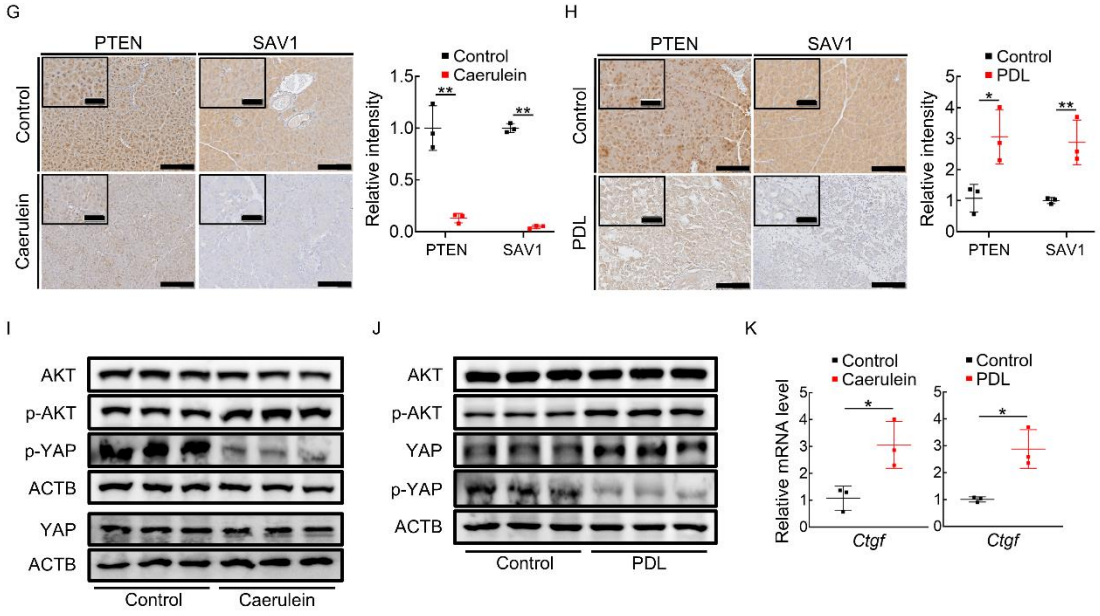

Figure 1

The expression of PTEN and SAV1 is downregulated in the pancreatic tissues of mice in two models of CP.

(G-H) Representative images of PTEN and SAV1 staining of pancreatic tissue in mice after repeated caerulein injection **(G left)** and quantification of the PTEN and SAV1 staining intensity **(G right)**, and in mice subjected to PDL surgery **(H left)** and quantification of PTEN and SAV1 staining intensity **(H right)**. **(I-J)** Protein levels of AKT, p-AKT, YAP, p-YAP, and ACTB in the pancreas of mice after repeated caerulein injection **(I)** and in mice subjected to PDL surgery **(J)**. **(K)** *Ctgf* mRNA levels in pancreatic tissue of mice after repeated caerulein injection **(left)** and in mice subjected to PDL surgery **(right).** Blots run in parallel contemporaneously or run at different times with loading control for each gel are shown. All data are presented as the means ± SDs of results for 3 mice per group. Student's t-test was used to evaluate differences between two groups. * $p < 0.05$ and ** $p < 0.005$. Scale bars: 100 μm and 50 μm (insets).

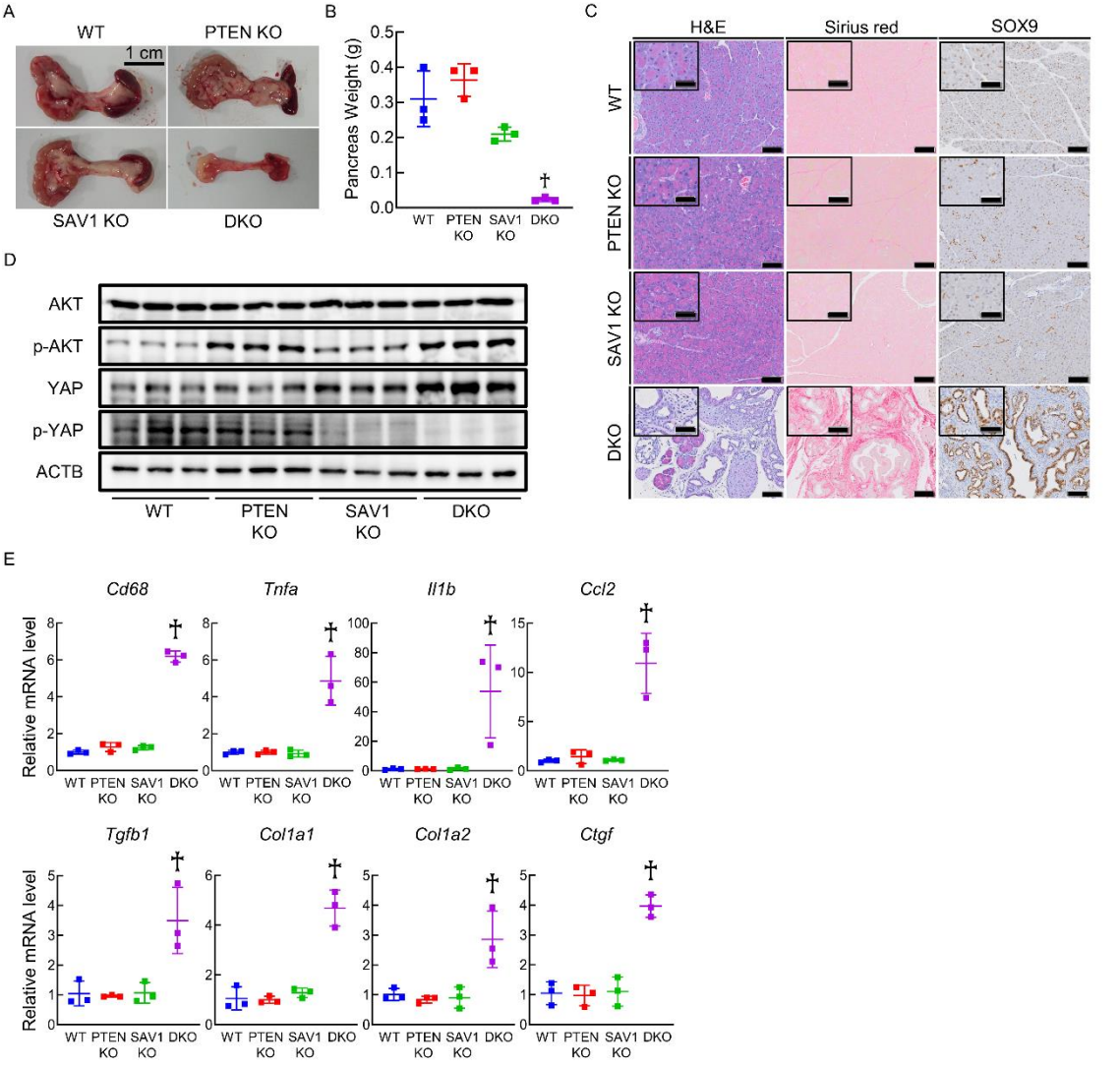

Figure 2

Mice with pancreas-specific loss of *Pten* and *Sav1* spontaneously develop CP.

Pancreatic phenotypes were examined in wild-type (WT) mice, pancreas-specific *Pten* knockout (KO) (PTEN KO) mice, *Sav1* KO (SAV1 KO) mice, and *Pten* and *Sav1* double KO (DKO) mice at 6 weeks of age. **(A)** Macroscopic images of the pancreas. **(B)** Pancreas weight. **(C)** Representative images of H&E, Sirius red, and SOX9 staining of pancreatic tissue. **(D)** Protein levels of AKT, p-AKT, YAP, p-YAP, and ACTB in the pancreas of mice. **(E)** *Cd68*, *Tnfa*, *Il1b*, *Ccl2*, *Tgfb1*, *Col1a1*, *Col1a2*, and *Ctgf* mRNA levels in pancreatic tissue. Blots run in parallel contemporaneously are shown. All data are presented as the means ± SDs of results for 3 mice per group. One-way analysis of variance (ANOVA) with Tukey's post hoc test was used to compare differences among four groups. † $p < 0.05$ versus all groups. Scale bars: 100 μm and 50 μm (insets).

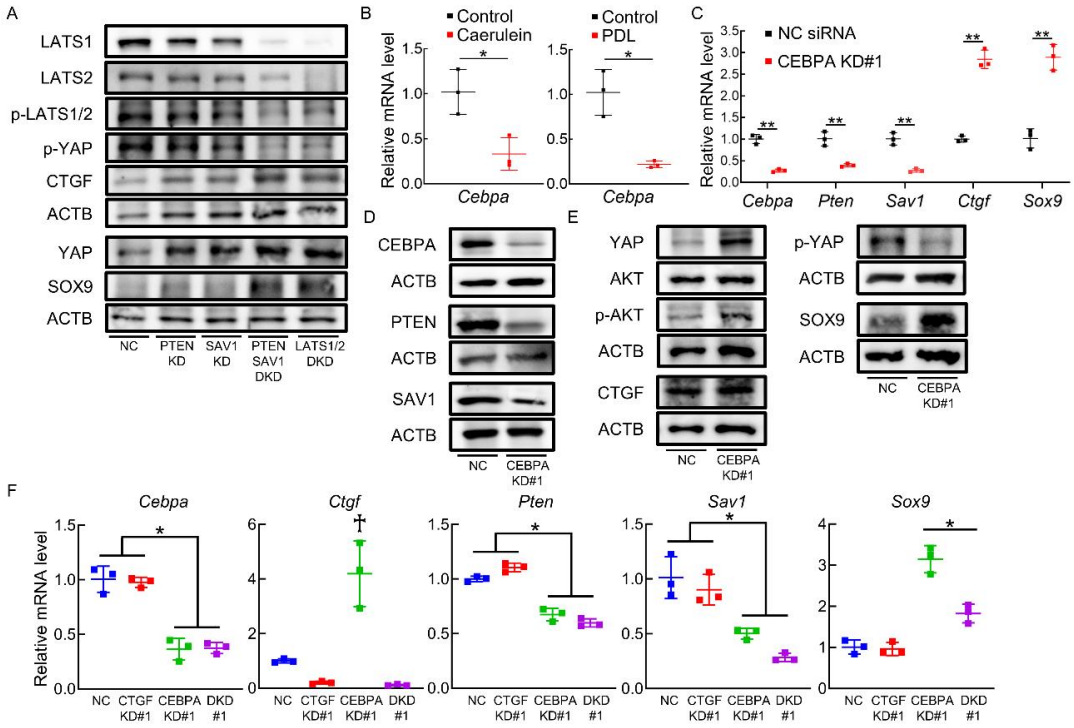

Figure 3

CEBPA positively regulates PTEN and SAV1 in acinar cells, and inhibition of PTEN and SAV1 induces ADM through CTGF upregulation in vitro.

(A) Protein levels of LATS1, LATS2, p-LATS1/2, YAP, p-YAP, CTGF, SOX9, and ACTB in 266-6 cells 3 days after transfection with negative control (NC) siRNA, *Pten* siRNA (PTEN knockdown [KD]), *Sav1* siRNA (SAV1 KD), both *Pten* and *Sav1* siRNAs (PTEN SAV1 double KD [DKD]), or both *Lats1* and *Lats2* siRNAs (LATS1/2 DKD). **(B)** *Cebpa* mRNA levels in pancreatic tissue in mice after repeated caerulein or vehicle (control) injections **(left)** and in mice subjected to PDL surgery or sham surgery **(right)**. **(C-D)** mRNA levels of *Cebpa*, *Pten*, *Sav1*, *Ctgf*, and *Sox9* **(C)** and protein levels of CEBPA, PTEN, SAV1, and ACTB **(D)** in 266-6 cells 3 days after transfection with NC siRNA or *Cebpa* siRNA (#1) (CEBPA KD#1). **(E)** Protein levels of YAP, p-YAP, AKT, p-AKT, CTGF, SOX9, and ACTB in 266-6 cells 3 days after transfection with NC siRNA or *Cebpa* siRNA (#1) (CEBPA KD#1). **(F)** mRNA levels of *Cebpa*, *Ctgf*, *Pten*, *Sav1*, and *Sox9* in 266-6 cells 3 days after transfection with NC siRNA, *Ctgf* siRNA (#1) (CTGF KD#1), *Cebpa* siRNA (#1) (CEBPA KD#1), or both *Cebpa* (#1) and *Ctgf* siRNAs (#1) (DKD#1). Blots run in parallel contemporaneously or run at different times with loading control for each gel are shown. The data are presented as the means ± SDs of results for 3 samples per group. Student's t-test was used to evaluate differences between two groups **(B and C)**. One-way analysis of variance (ANOVA) with Tukey's post hoc test was used to compare differences among four groups **(F)**. * $p < 0.05$, ** $p < 0.005$, and † $p < 0.05$ versus all groups.

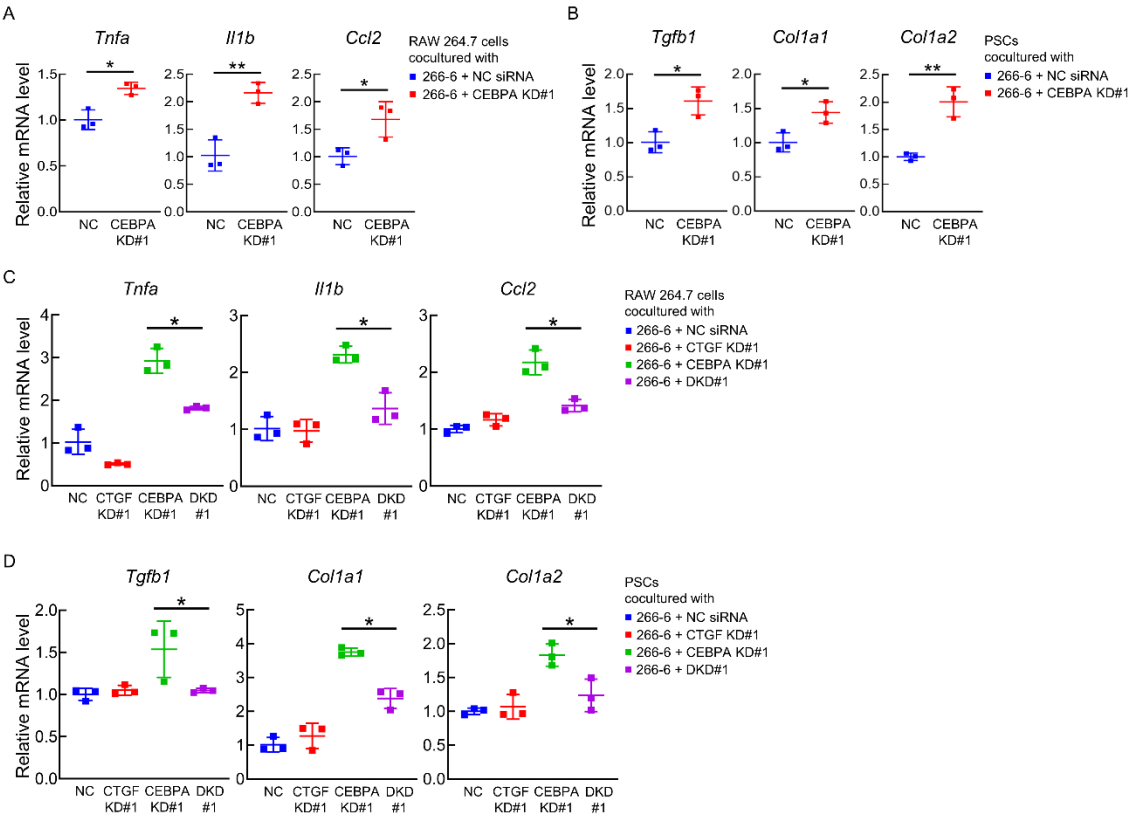

Figure 4

Inhibition of PTEN and SAV1 in PACs may activate surrounding macrophages and PSCs via CTGF upregulation in vitro.

(A) mRNA levels of *Tnfa*, *Il1b*, and *Ccl2* in RAW 264.7 cells 2 days after coculture with 266-6 cells transfected with negative control (NC) siRNA or *Cebpa* siRNA (#1) (CEBPA knockdown [KD] #1). **(B)** mRNA levels of *Tgfb1*, *Col1a1*, and *Col1a2* in PSCs isolated from mouse pancreata 2 days after coculture with 266-6 cells transfected with NC siRNA or *Cebpa* siRNA (#1) (CEBPA KD#1). **(C)** mRNA levels of *Tnfa*, *Il1b*, and *Ccl2* in RAW 264.7 cells 2 days after coculture with 266-6 cells transfected with NC siRNA, *Ctgf* siRNA (#1) (CTGF KD#1), *Cebpa* siRNA (#1) (CEBPA KD#1) or both *Cebpa* (#1) and *Ctgf* (#1) siRNAs (double KD [DKD] #1). **(D)** mRNA levels of *Tgfb1*, *Col1a1*, and *Col1a2* in PSCs isolated from mouse pancreata 2 days after coculture with 266-6 cells transfected with NC siRNA, *Ctgf* siRNA (#1) (CTGF KD#1), *Cebpa* siRNA (#1) (CEBPA KD#1) or both *Cebpa* (#1) and *Ctgf* (#1) siRNAs (DKD#1). All data are presented as the means ± SDs of results for 3 samples per group. Student's t-test was used to evaluate differences between two groups **(A and B)**. One-way analysis of variance (ANOVA) with Tukey's post hoc test was used to compare differences among four groups **(C and D)**. * $p < 0.05$ and ** $p < 0.005$.

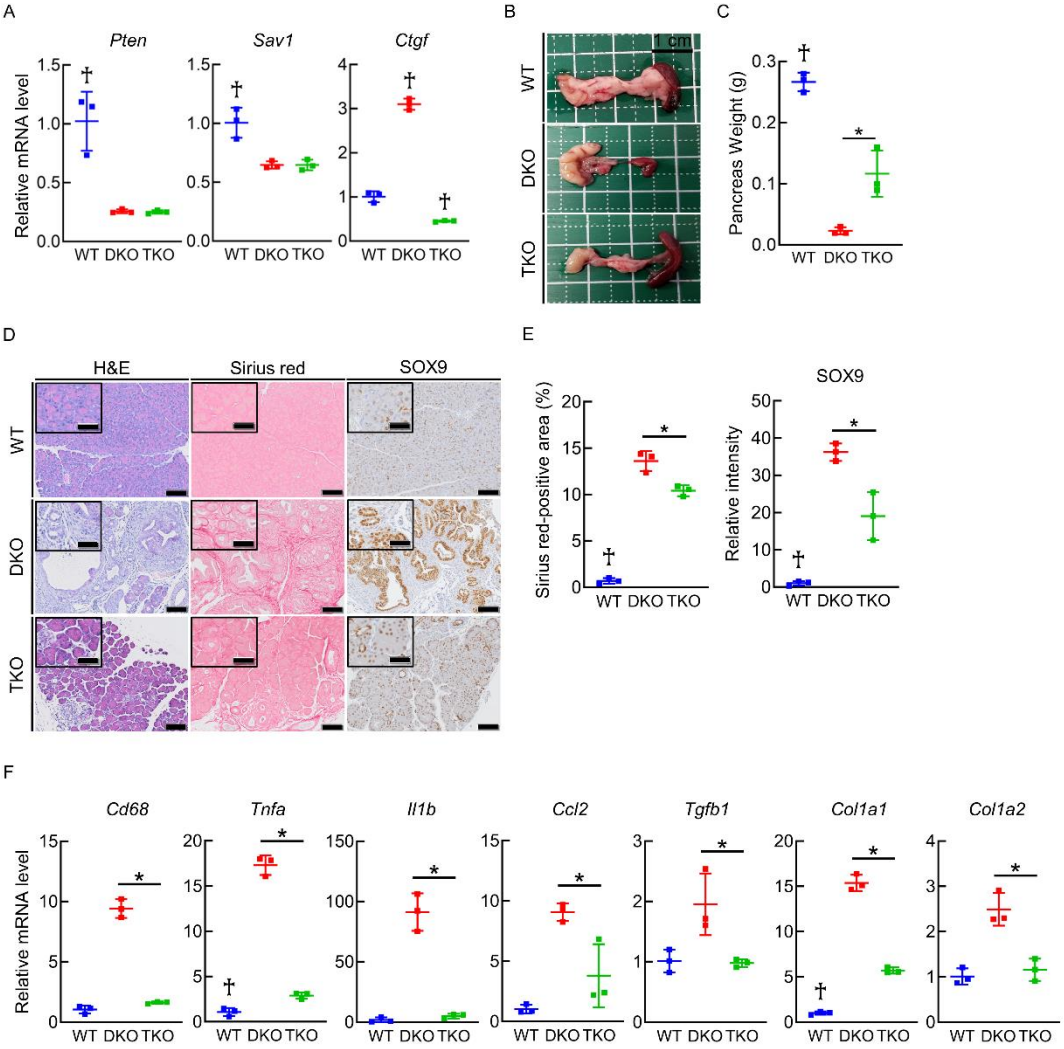

852
853 **Figure 5**

854 **CTGF produced by PACs is involved in the development of CP via pancreas-specific**
855 ***Pten* and *Sav1* loss in vivo.**

856 Pancreatic phenotypes were examined in wild-type (WT) mice, mice with pancreas-specific
857 *Pten* and *Sav1* double knockout (KO) (DKO), and mice with *Pten*, *Sav1*, and *Ctgf* triple KO
858 (TKO) at 6 weeks of age. **(A)** *Pten*, *Sav1*, and *Ctgf* mRNA levels in pancreatic tissue. **(B)**
859 Macroscopic images of the pancreas. **(C)** Pancreas weight. **(D-E)** Representative images of
860 H&E, Sirius red, and SOX9 staining of pancreatic tissue **(D)** and quantification of the Sirius
861 red-positive area **(E left)** and SOX9 staining intensity **(E right)**. **(F)** *Cd68*, *Tnfa*, *Il1b*, *Ccl2*,
862 *Tgfb1*, *Col1a1*, and *Col1a2* mRNA levels in pancreatic tissue. All data are presented as the
863 means ± SDs of results for 3 mice per group. One-way analysis of variance (ANOVA) with
864 Tukey's post hoc test was used to compare differences among three groups. * $p < 0.05$ and
865 † $p < 0.05$ versus all groups. Scale bars: 100 μm and 50 μm (insets).
866

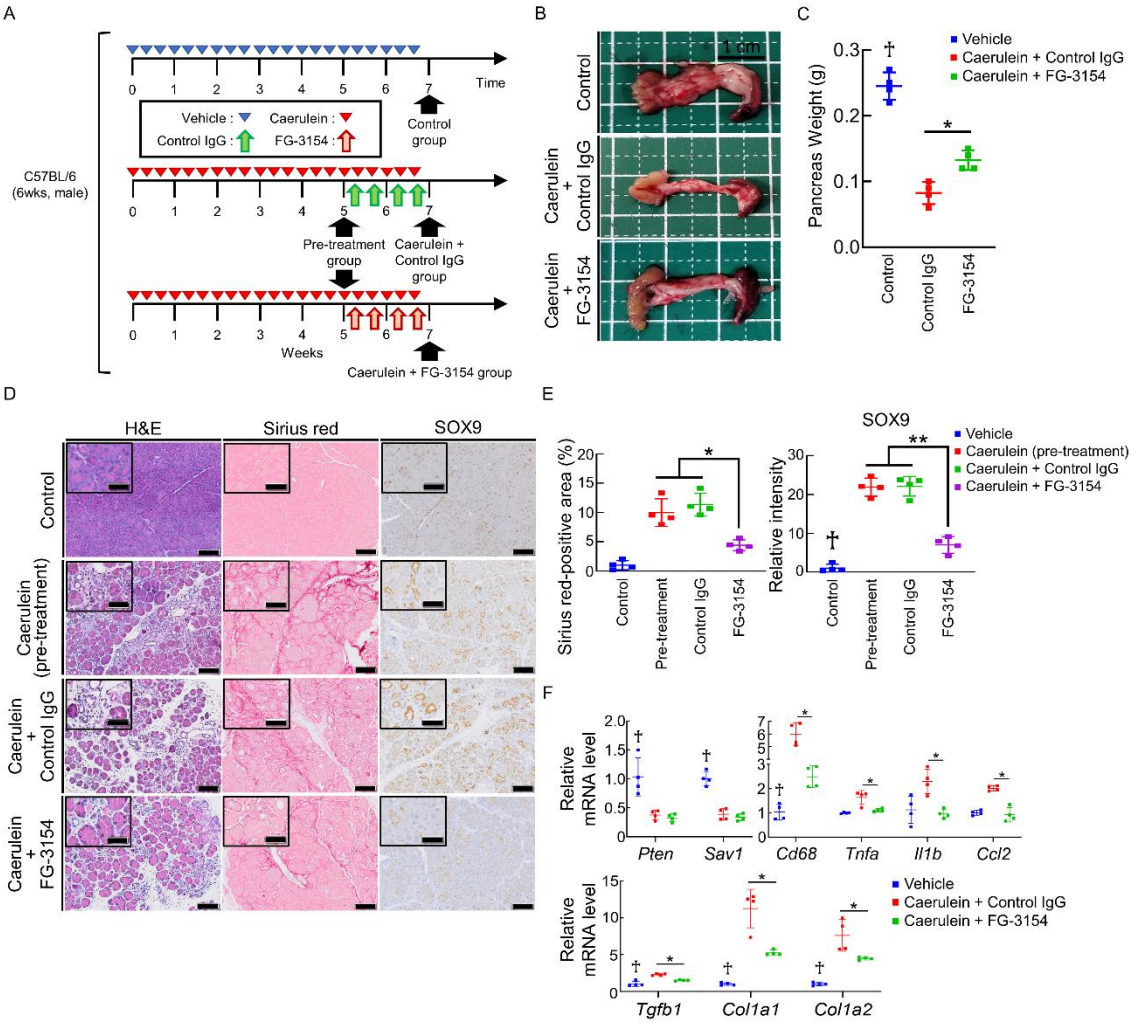

Figure 6

CTGF inhibition ameliorates CP by alleviating inflammation, fibrogenesis and ADM formation in vivo.

Pancreatic phenotypes were examined in vehicle-treated mice (control) and mice with caerulein-induced CP upon treatment with control IgG or FG-3154 (40 mg/kg) twice weekly for 2 weeks. **(A)** Therapeutic protocol. **(B)** Macroscopic images of the pancreas. **(C)** Pancreas weight. **(D-E)** Representative images of H&E, Sirius red, and SOX9 staining of pancreatic tissue **(D)** and quantification of the Sirius red-positive area **(E left)** and SOX9 staining intensity **(E right)**. **(F)** *Pten*, *Sav1*, *Cd68*, *Tnfa*, *Il1b*, *Ccl2*, *Tgfb1*, *Col1a1*, and *Col1a2* mRNA levels in pancreatic tissue. All data are presented as the means ± SDs of results for 4 mice per group. One-way analysis of variance (ANOVA) with Tukey's post hoc test was used to compare differences among three or four groups. * $p < 0.05$, ** $p < 0.005$, and † $p < 0.05$ versus all groups. Scale bars: 100 μm and 50 μm (insets).

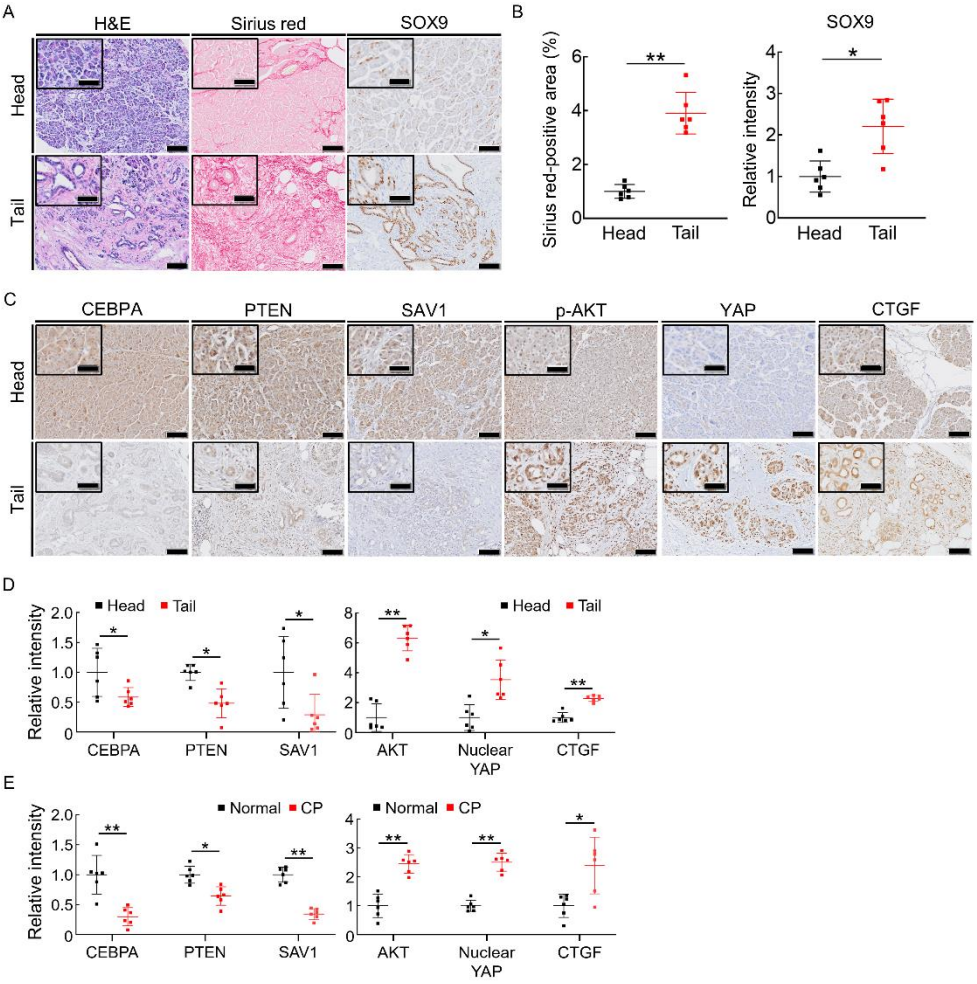

Figure 7

Chronic pancreatitis tissues exhibit lower PTEN and SAV1 levels and higher CTGF levels than nonpancreatitis tissues from humans.

(A-B) Representative images of H&E, Sirius red, and SOX9 staining of pancreatic tissue from the head or tail side of PDAC tumors from pancreatic cancer patients **(A)** and quantification of the Sirius red-positive area **(B left)** and SOX9 staining intensity **(B right)**. **(C-D)** Representative images of CEBPA, PTEN, SAV1, p-AKT, nuclear YAP, and CTGF staining of pancreatic tissue from the head or tail side of PDAC tumors from pancreatic cancer patients **(C)** and the relative staining intensity of CEBPA, PTEN, SAV1, p-AKT, nuclear YAP, and CTGF **(D)**. **(E)** The relative staining intensity of CEBPA, PTEN, SAV1, p-AKT, nuclear YAP, and CTGF staining of pancreatic tissue from the normal pancreatic regions obtained from pancreatic neuroendocrine tumor patients or from the chronic pancreatic regions obtained from chronic pancreatitis patients. All data are presented as the means ± SDs of results for 6 samples per group. Student's t-test was used to evaluate differences between two groups. * $p < 0.05$ and ** $p < 0.005$. Scale bars: 100 μm and 50 μm (insets).